I. ALIGNMENT FACTOR $\Delta A(r)$

To determine the degree of order we circularly integrate $g(r)$ weighted by $\cos(2\theta)$ and construct the order parameter ΔA.

$$\Delta A(r) = \int_0^{2\pi} g(r, \theta)\cos(2\theta)d\theta \quad (1)$$

where $g(r, \theta)$ is the pair correlation function in polar coordinate, and θ is the angle between r and the flow direction. The flow direction of interest is the averaged velocity direction $+45^\circ / -135^\circ$ since it sets the orientation of the shear induced string structure when the shear flow is linearly polarized. This order parameter is the real space analogue of the alignment factor, which has been used to quantify anisotropic suspension structures [3, 4]. ΔA is positive for flow-aligned structures and negative for vorticity-aligned structures. We calculate ΔA versus r/a for ten different values of δ, and plot the data for four values in Fig. 1. We find that for $\delta = 0$, ΔA has two negative extremes located at $r/a = 1.0$ and 2.1, corresponding to the vorticity-aligned structures. The sign of this functional form is opposite to the one found for flow-aligned structures [3, 4]. As δ_γ increases, the oscillation of ΔA decreases and becomes flat at $\delta_\gamma = \pi/2$.

We measure ΔA at the first and second negative peaks ΔA_1 and ΔA_2 and plot them versus δ_γ. We find that both ΔA_1 and ΔA_2 decay with increasing phase angle as illustrated in the inset of fig. 1. This gradual decrease indicates that the transition from the string phase to isotropic phase is continuous. We also find that ΔA_2 is smaller than ΔA_1 for all δ_γ. The ratio $\Delta A_1/\Delta A_2$ characterizes the probability ratio of finding a two-particle chain to that of a three-particle chain aligned along the vorticity direction. In combination with the real space images, these data demonstrate that as δ_γ is decreased, the particles form chains that are both long and kinked.

While the first and second local minimums of ΔA represent the distance between the nearest and second-nearest neighbors along the string direction respectively, the position of the local maximum characterizes the spacing between adjacent strings. We find that the position of the local maximum slightly increases from $r/a = 1.35$ to 1.45 as δ_γ increase from 0 to 0.70. This finding indicates that the spacing between strings slightly expands with increasing δ_γ. However, this string-string spacing becomes ill-defined as δ_γ approaches $\pi/2$ and string structure disappears.

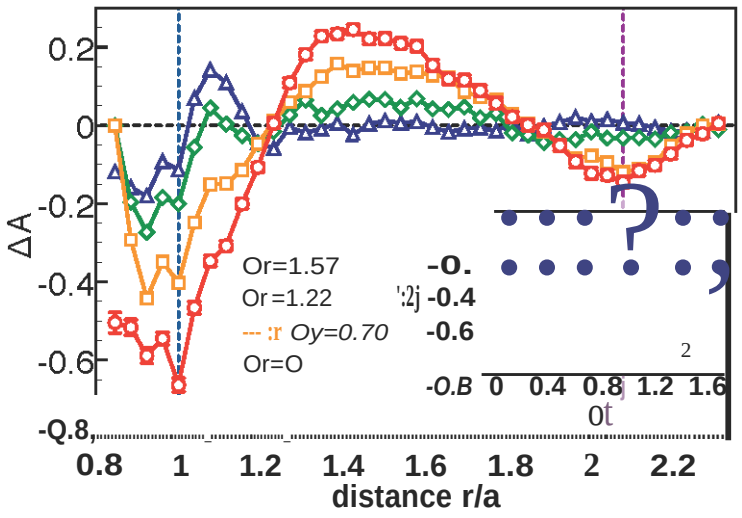

FIG. 1: Alignment factor $.6..A$ at four different li_1. At small phase angles, $.6..A$ oscillates and has two negative maxima at $r/a = 1$ (vertical left dashed line) and $r/a = 2.1$ (vertical right dashed line). The inset plots the alignment factors $.6..A1$ and $.6..A2$ versus $r5_1$.

II. TIME-DEPENDENT STRING ROTATION

In Fig. 2 of the main paper and Fig. 2 in the supplementary information, we find that as the phase angle 5_1 increases from 0 to $7r/2$, the particle configuration of the suspension transits from the string phase to the isotropic phase. These observed trends should be valid so long as the shear period is much smaller than the relaxation time. Stokesian Dynamics simulations[5-7] and previous experimental results[2], show that for the applied shear rate, the diffusivity is enhanced by a factor of 200. Thus, the time for a sheared sample to reach steady state is around $Te = Ts/200$ "" 0.3s where $Ts = 60$s is the relaxation time for the quiescent suspension. This shear-induced anisotropic diffusion enables particles to form strings within about one shear cycle when the shear frequency is high. To examine this microscopic mechanism and the timescale of string structure formation, we measure the time-dependent gxz under circularly polarized shear with two different sets of $(1_0, w)$. For the first measurement, we impose a shear flow with a small radius of gyration $/o = 2.5$ at high frequency $w = 31.4$s^{-1} (Fig 2(a)-(e)). The corresponding period of one shear cycle for the first measurement is $27r/w = 0.2$s. Consistent to our microscopic picture, we find that when the shear period is smaller than the estimated string formation time Te rv 0.3s, gxz is constantly isotropic over one cycle and independent of time(Fig 2(a)-(e)). For the second

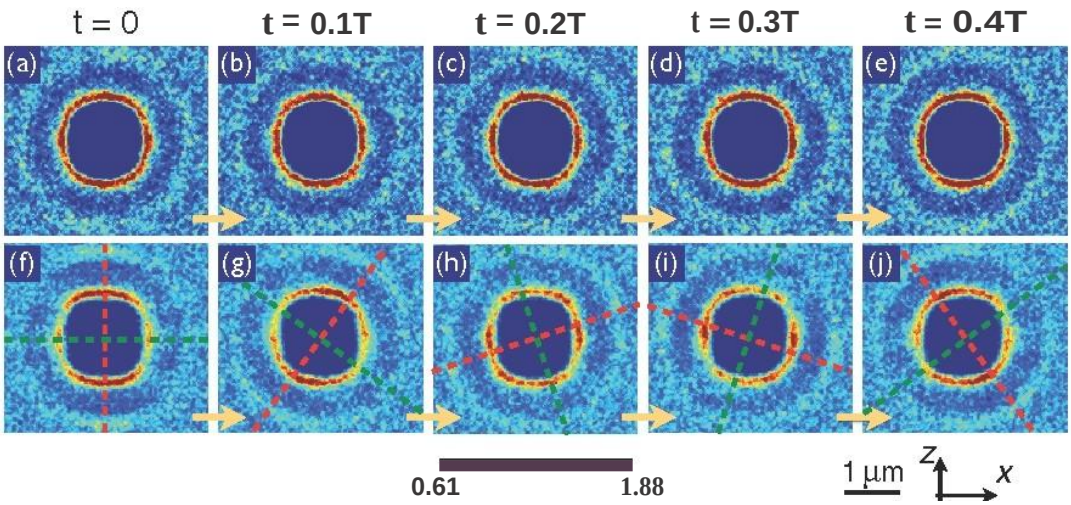

FIG. 2: Time dependent *gxz* over one cycle of shear for the $\Phi = 0.37$ sample at $\gamma_0 = 2.5$ (a)-(e) and $\gamma_0 = 12.5$ (f)-(j). The yellow arrows indicate the direction of time, where timet is normalized by the shear cycle period T. (a)-(e), *gxz* remains the same within one cycle. (f)-(j), anisotropy of *gxz* rotates with the shear flow. The relative orientation angle of the crosses in adjacent plots is $\pi/5$. The slight lag between the *gxz* anisotropy and the cross may be due to the finite scan rate of the confocal microscope.

measurement we impose a shear flow with a larger radius of gyration /o = 12.5 at a lower frequency $w = 6.3s^{-1}$ (Fig 2(f)-(j)). This circularly polarized shear flow shares the same shear rate of the previous circular flow since the value of /o x $w = 78.5s^{-1}$ is maintained. We find that when the shear period is increased to ls, which is beyond the string formation time T0.3s, *gxz* appears to exhibit a slight anisotropy that changes its orientation with the imposed flow reorientation(Fig 2(f)-(j)).

This observation of the time-dependent string structure provides further evidence that supports our microscopic picture of the string structure formation. Our results also demonstrates that a circularly polarized shear flow is able to either simply homogenize the in-plane structure or create cyclicly changing suspension morphology depending on the choice of the shear frequency *w*. Furthermore, the shear frequency can be characterized by the ratio between the shear period and the structure formation time, *Dee= 21rjwTe*. This dimensionless frequency is reminiscent of the Deborah number De=21r *jwTs* that compares the shear period and the suspension self-relaxation time.

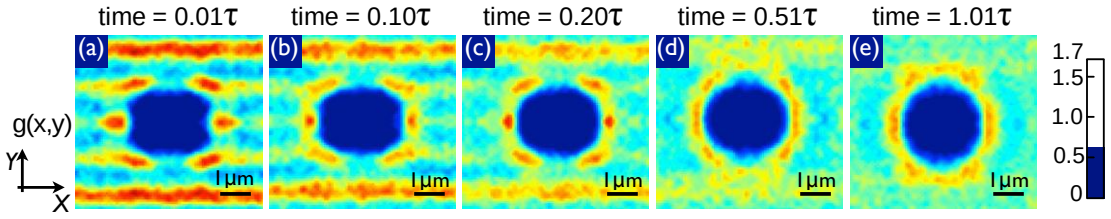

FIG. 3: Time series of the suspension g_{xy} after the cessation of the flow. The shear induced layer structure disappears at $t \approx \tau_s$. The data are averaged over five runs of the cessation measurements.

III. PHASE ANGLE DEPENDENCE: 3D STRUCTURE

In the main paper, we focus on the relation between the flow-vorticity plane particle configuration and the phase angel of imposed flow δ. In order to link the suspension structure to its rheological response, it is also important to investigate the particle configuration in the flow-gradient plane. In particular, we are interested in determining the shear induced layer structure [8]. Therefore, we image the three dimensional structure of confined suspensions under biaxial shear for different δ.

A. Structure Relaxation

In our experiments, a high shear rate is required to generate the string structure [2]. This high shear rate $\dot{\gamma} \sim 100s^{-1}$ prohibits real-time 3D scanning while the sample is simultaneously sheared. Fortunately, due to the very low Reynolds number $\mathrm{Re} \sim 10^{-6}$, and the long relaxation time $\tau_s \sim 60s$ of the confined system, the suspension structure remains nearly the same for a reasonably long period after shear cessation. However, it is still important to experimentally determine the relaxation time of the shear induced structure. Therefore, with our high-speed confocal microscope, we image the suspension 3D structure immediately after the cessation of the shear flow with a scan rate of one stack per second. After featuring the particle positions from a 3D image stack, we calculate the *in situ* $g_{xy}(t)$ by taking a cross section of $g(r,t)$ centered at $z = 0$ with a width of $2.5\mu m$. We show a series of $g_{xy}(t)$ in the time interval $0.01\tau_s \leq t \leq 1.01\tau_s$ in Fig. 3, where $t = 0$ denotes the cessation time of the shear flow. At $t = 0.01\tau_s$, $g_{xy}(0.01\tau_s)$ shows a pronounced layer configuration as indicated by the horizontal stripes (Fig. 3(a)). As time increases, we find that the shear induced layering gradually disappears (Fig. 3(b)-(e)). For times longer than τ_s, we still observe a

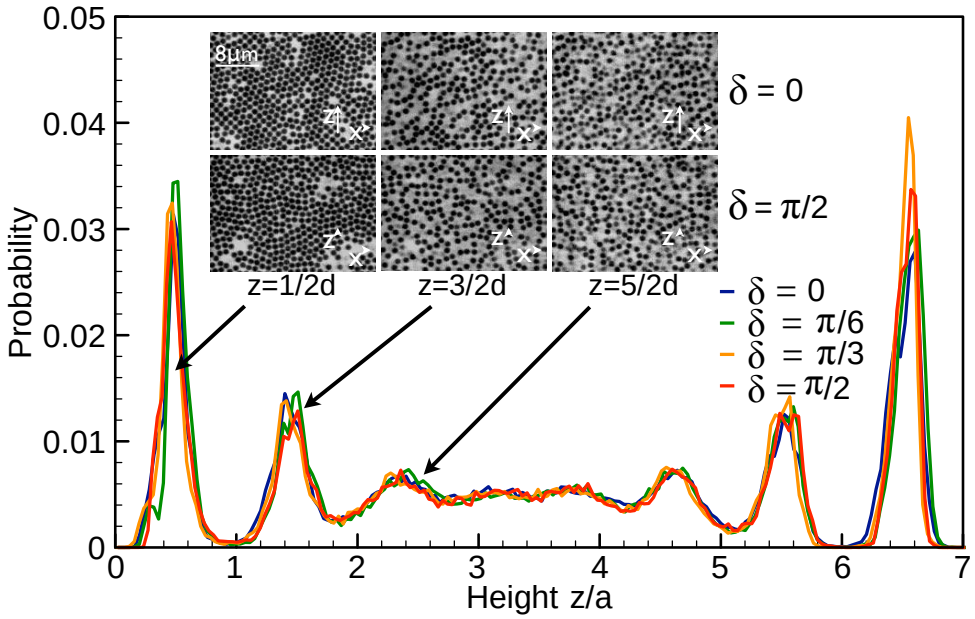

FIG. 4: Particle density profile for four different values of δ and the confocal images of the suspension at different height. The top and bottom rows of images illustrate the cases for $\delta = 0$ and $\delta = \pi/2$ respectively.

weak order structure which should arise from the particle packing and geometric constraint of confinement (Fig. 3(e)).

To understand the underlying mechanism of the layer structure formation, we compare our observations with the results from the literature [8]. Previous simulations have shown that in a confined suspension, the confinement-induced hydrodynamic mechanism prevents the particle swapping in adjacent streamlines, and results in a pronouced non-equilibrium layer structure[8]. Our observations of the layer structure for an intermediate volume fraction $\varphi = 0.37$ is consistent with the results simulated for the dilute-suspension limit[8]. Furthermore, the reversed isotropic phase of the suspension (Fig. 3(e)) also rules out the possibility that the string structure is generated through the Van der Waals force between particles. Since the energy scale of Van der Waals force between silica colloids is significantly higher than the thermal energy, sonication is typically the only way to separate particles that are bonded by such a strong attractive forces. In summary, this observation shows that the vorticity-aligned strings in our confined system arise from the hydrodynamic interactions[2] rather than interparticle attractions[9, 10].

B. Layer Structure

To investigate the relation between the layer structure and phase angle δ_γ, we calculate the particle density profile along the Y-axis (gradient axis), and plot the distribution function for four different $\delta_\gamma = 0, \pi/6, \pi/3,$ and $\pi/2$ in Fig. 4. To obtain better statistics while still accurately capturing the instantaneous structure immediately after flow cessation, each distribution function is averaged over time with an interval $0.01\tau_s \leq t \leq 0.08\tau_s$ and five separate runs of measurements. We find visually indistinguishable density profiles for all δ_γ, where the layering order is the highest near the wall and lower in the bulk of the sample. The shape of the density profiles in our experiments is consistent with the results previously simulated in hydrodynamic systems[8]. The quantitatively similar density profiles and the pronounced layer structure imply a low interlayer swapping rate of particles at all δ_γ in our confined suspensions. These results also suggest that all particle layers simply slide back and forth under oscillatory shear for all δ_γ. The 3D image stacks also allow us to examine the particle configuration in the $X-Z$ plane at different heights. The six sub-figures in Fig. 4 show the confocal images of the suspension at three different heights $z/a = 0.5, 1.5,$ and 2.5. String structure can still be observed in the middle of the suspension ($z/a = 2.5$) for $\delta_\gamma = 0$ despite the relatively lower local volume fraction (upper right panel). The particles in the very top and bottom layers assemble into crystal structure with or without a universal orientation for $\delta_\gamma = 0$ or $\pi/2$ respectively.

As indicated by the symmetric density profiles in Fig. 4, it is surprising that there is nearly no decay of the particle density due to sedimentation although the density mismatch between the particle and solvent is $\approx$50%. This observation shows that the particle-particle and particle-wall hydrodynamic interactions dominate over gravitational force and effectively resuspend the suspension along Y-axis. This finding in conjunction with the observed isotropic state for $\delta_\gamma = \pi/2$, shows that for high De_e circularly-polarized shear flow the particles remain suspended while the in-plane structure remains isotropic.

[1] R. Pasquino, F. Snijkers, N. Grizzuti, J. Vermant, Rheologica Acta, 2010, **49**, 993-1001.

[2] B. J. Maranzano and N. J. Wagner, J. Chem. Phys., 2002, **117** 10291-10302.

[3] D. R. Foss, and J. F. Brady, J. Fluid Mech., 1999, **401**, 243-274.

[4] A. Acrivos, J. Rheol., 1995, **39**, 813-826.

[5] A. Sierou, J. F. Brady, J. Fluid Mech., 2004, **506**, 285-314.

[6] M. Zurita-Gotor, J. B?awzdziewicz, and E. Wajnry, Phys. Rev. Lett., 2012, **108**, 068301

[7] C. O. Osuji, D. A. Weitz, Soft Matter, 2008, **4**, 1388-1392.

[8] A. Montesi, A. A. Pea, and M. Pasquali, Phys. Rev. Lett., 2004, **92**, 058303.